High pressure-temperature Raman measurements of H_2O melting to 22 GPa and 900 K

Jung-Fu Lin, Burkhard Militzer, Viktor V. Struzhkin, Eugene Gregoryanz, Russell J. Hemley, and Ho-kwang Mao
Geophysical Laboratory, Carnegie Institution of Washington, Washington, DC 20015

(Received 12 May 2004; accepted 25 June 2004)

The melting curve of H_2O has been measured by *in situ* Raman spectroscopy in an externally heated diamond anvil cell up to 22 GPa and 900 K. The Raman-active OH-stretching bands and the translational modes of H_2O as well as optical observations are used to directly and reliably detect melting in ice VII. The observed melting temperatures are higher than previously reported x-ray measurements and significantly lower than recent laser-heating determinations. However, our results are in accord with earlier optical determinations. The frequencies and intensities of the OH-stretching peaks change significantly across the melting line while the translational mode disappears altogether in the liquid phase. The observed OH-stretching bands of liquid water at high pressure are very similar to those obtained in shock-wave Raman measurements.
 [DOI: 10.1063/1.1784438]

I. INTRODUCTION

The properties and phase diagram of H_2O at high pressure and temperature are of fundamental interest in physics, chemistry, and planetary sciences. Many properties of water have yet to be characterized accurately under extreme conditions, and experimental data are needed to test theoretical predictions. In particular, characterization of water is crucial for identifying and understanding numerous chemical reactions at extreme conditions where the state of water changes from hydrogen-bonded to dissociation dominated. The melting curve and equation of state (EOS) of H_2O at high pressure is also important in planetary science, specifically for our understanding of the internal properties and composition of planets. Ice is assumed to be a major component of the interior of Uranus and Neptune as well as in Jupiter's icy satellites.[1–3]

Shock-wave experiments have served as the main tool to characterize fluid water at high pressures. The results have been used to derive and to constrain a variety of EOS models.[4–9] Shock-wave studies have also provided additional measurements of water at high pressures such as Raman spectra[10] and electrical conductivity.[5,11] These experiments suggest that high pressure-temperature (P-T) conditions generate highly mobile charge carriers through molecular dissociation leading to an increase in conductivity.[5,10,11] The observed changes in the microscopic structure of water put a limit on the validity of a whole class of classical water models, which are based on interacting but intact molecules. In contrast, *ab initio* theoretical approaches are not limited in this respect and have been used to characterize dissociation processes in water under pressure.[12–13] *Ab initio* simulations by Cavazzoni *et al.*[14] have challenged the established understanding of the high-pressure melting mechanism by predicting the existence of an intermediate superionic regime that governs the transition from solid to liquid water above 30 GPa. However, high P-T protonic diffusion experiments of H_2O and D_2O in ice VII reported to date indicate that the diffusion coefficients close to the melting curve of ice VII are less by two to three orders than expected for superionicity.[15]

In comparison to shock-wave and theoretical studies, only a few static high P-T experiments on H_2O have been reported. However, the experimental results obtained with different physical phenomena used in detecting melting are not consistent, leading to very different predictions for the ice VII melting curve.[16–21] The appearance and disappearance of the energy-dispersive x-ray diffraction peaks were used to detect melting in ice VII up to 40 GPa in an externally heated diamond anvil cell (EHDAC).[18,21] These results are in good agreement with resistivity-based melting measurements in a large volume press,[16,17] where a drop in electrical resistance was used to infer melting. However, the addition of other materials to increase the resistivity of the sample may have led to melting point suppression in compressed H_2O. Optical observation of melting in ice VII by Datchi *et al.*[19] provided data up to 13 GPa and raised questions about the validity of previous x-ray diffraction measurements. Their experiments predicted significantly higher melting temperatures; e.g., at 13 GPa, Fei *et al.*[18] and Frank *et al.*[21] measured a melting temperature of 670 K whereas Datchi *et al.*[19] reported 750 K. Furthermore, the reported slope of the melting line is very different, which leads to substantial deviations when the melting line is extrapolated to higher pressures.[18,19,21] On the other hand, angle-dispersive x-ray diffraction has been used recently to detect melting of ice VII up to 40 GPa.[15] The derived melting curve lies between previous energy-dispersive x-ray diffraction[18,21] and optical results.[19] The melting curve of H_2O has also been measured in a laser-heated diamond cell using optical observation of the laser-speckle pattern of an Ar^+ laser line in which H_2O was mixed with metal powder as a laser absorber in the range of 20–90 GPa and 1000–2400 K.[22] The melting

line was reported to be much higher than in all previous studies.

Given this controversy between previous results from different experimental techniques used in detecting melting in H_2O, we have carried out *in situ* Raman measurements in an EHDAC as a direct technique to detect melting of ice VII at high pressure. The disappearance of the translational mode and dramatic changes in OH-stretching bands across melting together with the optical observation of melting are used to distinguish ice VII and liquid H_2O. Close to the melting line we found ice VII to recrystallize in different orientations as the pressure and temperature were varied,[23] which makes it difficult to identify the ice phase in x-ray diffraction experiments. This indicates that x-ray diffraction technique may provide only a lower bound on the melting curve.

II. EXPERIMENTAL METHODS

Distilled and deionized H_2O sample was loaded into the sample chamber of an EHDAC (Ref. 24) with flat diamonds with the culet size of 400–700 μm. A Re gasket was preindented to a thickness of 30 μm and a hole of 100 μm was drilled in the very center of the preindented area, ensuring the reliability of the pressure correction. A smaller hole of 20 μm in diameter was drilled near the sample chamber and filled with Sm:YAG (YAG—yttrium aluminum garnet) as a pressure calibrant at high temperatures,[25] because Sm:YAG is known to dissolve in water above 600 K.[19] Since the pressure calibrant was not placed in the sample chamber, test experiments were performed by placing Sm:YAG and ruby chips in both chambers up to ~650 K to correct the pressure difference which was about 10% from 300 to ~650 K; the 10% pressure correction was assumed to be valid at higher temperatures. Tungsten carbide seats with chromel wires were used as external heaters whereas inert gas of Ar with 2% H_2 was flowed into the EHDAC to provide a reduced environment and to protect the heaters and diamonds. Temperatures were controlled by a feedback power supply with uncertainties of less than 10 K and measured from two K-type thermocouples attached to the diamond surfaces or from one R-type thermocouple placed between diamonds.[24] In some of the experiments, we also used a small Au liner inserted in the drilled hole of the Re gasket to confine the H_2O sample and to test for potential chemical reaction; we found no evidence of chemical reactions between the Au or Re gasket and H_2O sample. The 488 or 514 nm line of an Ar^+ laser was used as the Raman excitation source and Raman spectra were collected by an HR-460 spectrograph with a charge-coupled device (CCD). Both high- and low-resolution gratings (300 and 1800 g/mm) were used for recording the OH-stretching and low-frequency translational bands.

III. RESULTS AND DISCUSSION

Raman spectra of H_2O were measured up to 32 GPa and 1100 K. Figure 1 shows a series of Raman spectra for the Raman-active translational modes at different P-T conditions obtained during one heating cycle in which the temperature was stepwise increased above the melting line and then lowered. Coinciding with optical detection of melting, the translational bands disappear. Consequently, the observation of the translational modes can be used as an indication for the presence of ice VII and its disappearance suggests the occurrence of liquid H_2O.[26–33]

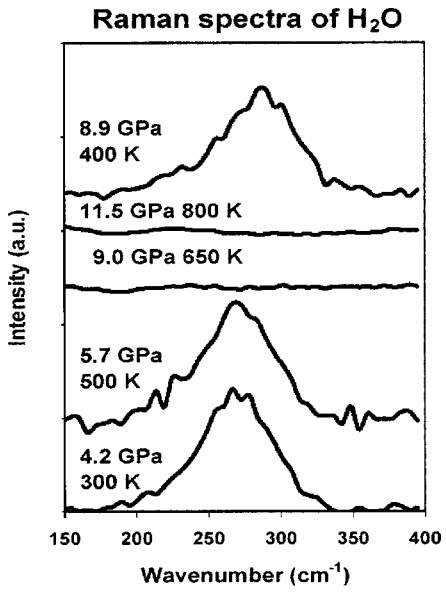

FIG. 1. Representative Raman spectra of the translational mode of H_2O at various P-T conditions. The translational mode was clearly observed in solid ice VII whereas it disappeared in liquid H_2O.

Figure 2 shows OH-stretching bands at the same P-T conditions. The intensities are about one order of magnitude higher than the translational modes. In the solid phase, one can identify the A_{1g} and B_1 peaks of ice VII while the E_g peak is too weak to be resolved at temperatures above ~500 K.[26–33] The widths of both peaks increase with temperature while the frequencies decrease with pressure and increase with temperature. We further observed that the magnitude of the frequency shift with pressure decreases at higher temperatures. As the temperature is raised above the melting line, the spectra in the region of OH-stretching bands change significantly; in particular, the relative intensities of the two main features are reversed (see Figs. 2 and 3 for more details). The changes are consistent with the disappearance of the lattice mode excitations and can be used as a third criterion to infer melting. At pressures above ~20 GPa, the OH-stretching modes overlap with the second-order Raman signal from the diamond anvils, making it difficult to use these modes to detect melting. Nevertheless, the translational mode can still be used to detect melting. At temperatures close to the melting curve, we optically observed the formation of ice crystals while the OH-stretching and translational bands clearly showed the presence of the ice VII. This suggests that the melting line measured previously by x-ray diffraction[18,20,21] provide only a lower bound for the melting temperature.

Our Raman spectra of liquid H_2O are very similar to those obtained in shock-wave measurements reaching 26 GPa and 1700 K.[10] These Raman spectra have been explained in terms of a two-component mixture model predict-

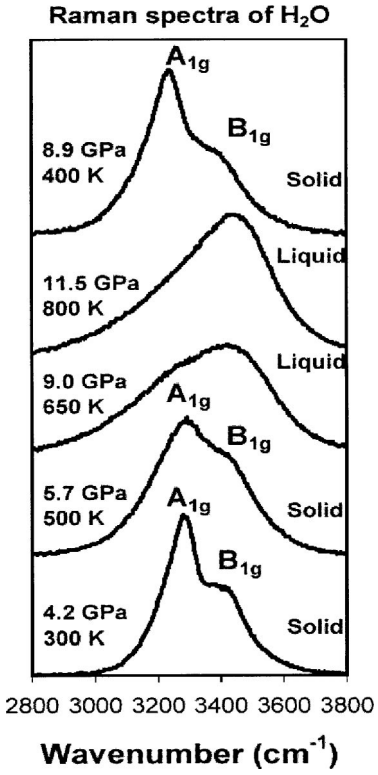

FIG. 2. Representative Raman spectra of the OH-stretching modes for P-T conditions corresponding to Fig. 1. The stretching modes change significantly across melting (see Fig. 3); the low-frequency A_{1g} mode is the dominant peak in ice VII while the high-frequency mode dominates in liquid water.

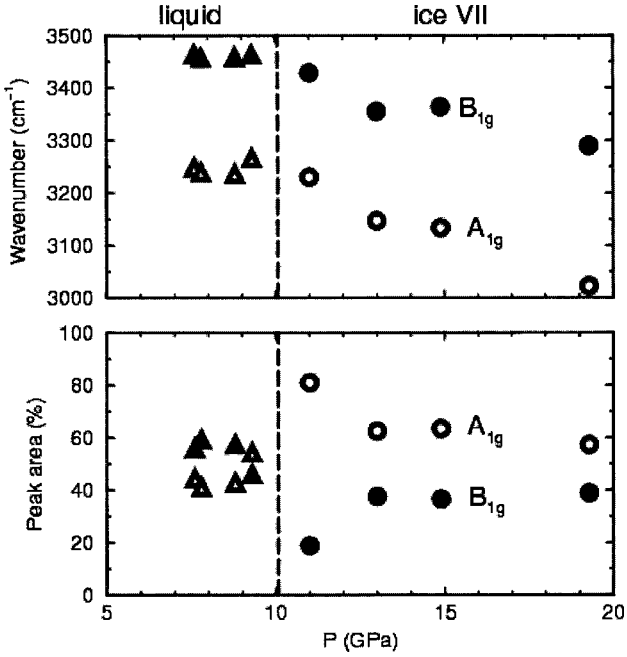

FIG. 3. Pressure dependence of the frequencies and the integrated intensities of the OH-stretching bands at 700 K. Two OH-stretching bands, A_{1g} and B_{1g}, are observed in ice VII as the E_g band is too weak to be distinguishable from other bands. The Raman spectra have been fitted to a two-component model in Voigt functions (open triangles: low-frequency band and solid triangles: high-frequency band) as that best described both solid and liquid Raman patterns and allowed us to quantitatively describe the changes in the peak intensity. OH modes in liquid H_2O are depicted as triangles, whereas circles are used for the solid phase: H_2O-ice VII. Open symbols refer to the low-frequency OH band, and solid symbols indicate the higher frequency band. At melting [indicated by dashed line corresponding to Eq. (1)], the ordering of the peak intensities is reversed (lower plot) (also see Fig. 2).

ing two bands: an essentially free, monomeric OH-stretching band at higher frequency and the strongly hydrogen-bonded band at lower frequency.[10] The increase in intensity in the high frequency band was interpreted as an indication for the dominant presence of H^+ and OH^- ions in hot dense water.[10] However, a series of *ab initio* molecular dynamics simulations at similar thermodynamic conditions found that the dissociation of water occurs through a bimolecular process similar to ambient conditions, leading to the formation of short-lived OH^- and H_3O^+ ions.[13,14] Since our Raman spectra did not show any clear signature of a band associated with a high concentration of ionic species[34] (OH^- and H_3O^+), we cannot draw any conclusions about the dissociation mechanism in water at high P-T conditions.

We fitted the Raman spectra to a two-component mixture model with Voigt functions as we found that this best described both the solid and liquid spectra (Fig. 3). As shown, the intensities of the bands are reversed across melting; the low-frequency A_{1g} mode is the dominant band in the solid phase while the high-frequency mode, presumably the free OH-stretching band, is the dominant feature providing a strong indication of melting. The intensity of the low-frequency A_{1g} mode increases with increasing temperature and decreasing pressure. The relative intensity of the high-frequency band in water increases with rising temperature up to 1100 K, consistent with shock-wave experiments.[10]

The Raman measurements were performed up to 32 GPa in pressure and 1100 K in temperature (Fig. 4). Data in the vicinity of the melting line were collected up to 22 GPa and 900 K. Although other melting laws can be applied,[19,35] we find that the melting data are well described by the following Simon-Glatzel equation,[36]

$$\frac{P-P_t}{P_C}=\left(\frac{T}{T_t}\right)^a-1, \tag{1}$$

where $P_t=2.17$ GPa and $T_t=355$ K characterize the ice VI-VII-liquid triple point. The fit parameters $P_C=0.85$ GPa and $\alpha=3.47$ were obtained by the following algorithm that directly uses two sets of measured P-T points, one set for the liquid and one for the solid phase. Ideally, the fitted melting line should be above all *solid* points and below all points characterized as *liquid*. However, because of the uncertainty of the P and T measurements a small number of P-T points lie on the opposite side of the best possible fit of the melting curve. The following fit algorithm derives the parameters P_C and α by minimizing the number of points that lie on the wrong side of the melting curve. (The algorithm does not actually require any data points on the opposite side.) More specifically, it minimizes the *probability* that a data point labeled as solid is above the melting line and that a point characterized as liquid is below. To estimate the probability density in P-T space for the exact location of data point, we center a two-dimensional Gaussian error function around each measured P-T data point. The widths are given by the

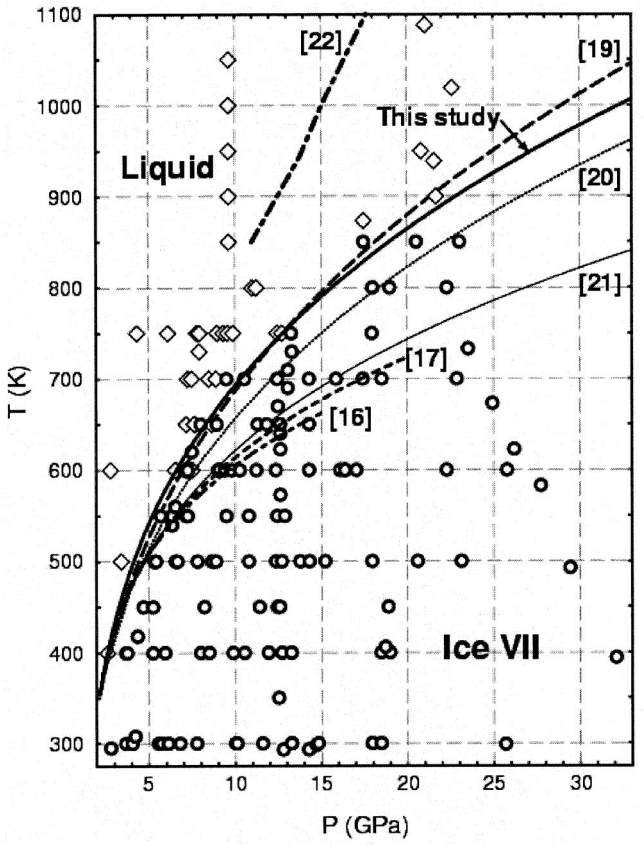

FIG. 4. Melting curve of ice VII at high P-T. Circles and diamonds represent Raman measurements in the solid and liquid phases, respectively. The uncertainties in pressure and temperature are approximately 5% and 10 K, respectively. The melting curve (solid line) obtained by fitting our results to the Simon-Glatzel equation (Ref. 36) is compared to previous melting studies [ordered with decreasing temperature]: Schwager *et al.* (filled squares) (Ref. 22), Datchi *et al.* (long dashed line) (Ref. 19), Dubrovinskaia and Dubrovinsky (dotted line) (Ref. 20), Frank *et al.* (thin solid line) (Ref. 21), Mishima and Endo (dashed line) (Ref. 17), and Pistorius *et al.* (dot-dashed line) (Ref. 16). We note that the melting curve of Schwager *et al.* was constructed by extrapolating their data back from pressures above 15 GPa and temperatures above 1050 K.

experimental error bars in pressure ($\pm 5\%$) and temperature (± 10 K). We then integrate over the P-T space strictly above a proposed melting line and add the contributions from all Gaussians in the solid data set. Similarly, we integrate the P-T space below the melting line and add the contribution from the liquid data set. The smaller the sum of both integrals, the more realistic is the fit. This sum is then minimized with respect to P_C and α, which provides us with a simple and robust method to fit a melting line in cases where a direct determination of the melting line is impractical and only P-T points in the vicinity are available. An extension to other melting laws is straightforward. The resulting melting law shown in Fig. 4.

Our melting line is in good agreement with measurements up to 13 GPa by Datchi *et al.*,[19] who combined optical observation of melting with quasi-isochoric P-T scans. The observed melting temperatures are significantly higher than those obtained from the disappearance of the x-ray diffraction peaks in ice VII using the EOS of Au as an internal pressure calibrant.[18,20,21] In those experiments, it is possible that as large crystallites of ice VII form in different orientations as P-T points were increased, thereby causing a loss in the powder diffraction pattern. Indeed, we optically observed this recrystallization phenomenon in our experiments, and such recrystallization is also documented in previous experiments.[23] This recrystallization can lead to a loss of diffraction peaks in an energy-dispersive measurement. Since it is likely that the area detectors used in angle-dispersive diffraction experiments only allows one to identify some but not all recrystallization processes, previous x-ray melting lines should be considered as a lower bound for the melting line.[18,20,21] Thus, the observation of diffuse scatter with an area detector from liquid water would provide important criteria to indicate melting. Moreover, one can also use Laue diffraction with a white x-ray beam to detect diffraction signals from single-crystal ice. The use of MgO in H_2O in the experiments by Frank *et al.*[2] could also cause the depression of the melting curve of H_2O and hence give a lower melting line. Nevertheless, unit-cell volume measurements for the ice VII phase remain valid and can be combined with the corrected melting line for further EOS calculations.

Recent angle-dispersive x-ray diffraction measurements by Dubrovinskaia and Dubrovinsky[20] using an area detector gave a melting between our results and those from energy-dispersive x-ray measurements. The difference between our measurements and those of Dubrovinskaia and Dubrovinsky[20] can partly be attributed to different pressure calibrants (Sm:YAG versus Au). The phase transformation from ice VII to ice X would change the slope of the extrapolated melting curve, increasing the melting point at higher pressures.[22,32,33] A distinct change in melting slope at about 43 GPa and 1600 K has been reported as a first-order transformation from ice VII to ice X, though the melting curve was much higher than all other studies.[22] Recent *in situ* high P-T Raman measurements of solid CO_2 in a laser-heated DAC showed that the sample temperature was lower than the surface temperature when a metallic laser coupler is used;[37,38] this result suggests that the melting curve reported by Schwager *et al.*[22] should be corrected downward. The phase diagram of H_2O at these high P-T conditions remains to be explored. *In situ* Raman spectroscopy with EHDACs and laser-heated DACs[37–39] provides a useful combination of techniques for characterizing the properties and phase diagram of H_2O under these conditions.

IV. CONCLUSIONS

We report *in situ* Raman measurements that provide a direct and reliable determination of melting high P-T phase behavior of H_2O. The disappearance of the translational mode and changes in the OH-stretching bands were combined with optical observations to determine the melting line of ice VII up to 22 GPa. The results obtained are in good agreement with previous optical measurements[19] but differ from previous x-ray diffraction and laser-heating results.[18,20,21] Although the OH-stretching bands overlap with the second-order Raman bands of the diamond anvils above $\sim$20 GPa, the observation of the translational mode provides a reliable way of detecting melting at higher pressures where other phases are predicted. *In situ* Raman measurements rep-

resent a powerful technique to characterize the high *P-T* properties of other important molecular components present in planetary interiors such as H_2, NH_3, and NH_4.

ACKNOWLEDGMENTS

The authors thank M. Santoro, Y. Fei, H. Scott, and S. Gramsch for their help and comments. The authors also thank W. A. Bassett and I. M. Chou for helpful discussions and technical assistance. V.V.S. acknowledges financial support from the Department of Energy under Grant No. DE-FG02-02ER45955. This work was supported by DOE/BES, DOE/NNSA (CDAC; Grant No. DE-FC03-03NA00144), NASA, NSF, and the W.M. Keck Foundation.

[1] G. J. Consolmagno and J. S. Lewis, Icarus **34**, 280 (1976).
[2] J. D. Anderson *et al.*, Science **280**, 1573 (1998).
[3] H. P. Scott, Q. Williams, and F. J. Ryerson, Earth Planet. Sci. Lett. **203**, 399 (2002).
[4] M. H. Rice and J. M. Walsh, J. Chem. Phys. **26**, 824 (1957).
[5] A. C. Mitchell and W. J. Nellis, J. Chem. Phys. **76**, 6273 (1982).
[6] S. K. Saxena and Y. Fei, Geochim. Cosmochim. Acta **51**, 783 (1987).
[7] A. Belonoshko and S. K. Saxena, Geochim. Cosmochim. Acta **55**, 381 (1991).
[8] K. S. Pitzer and S. M. Sterner, J. Chem. Phys. **101**, 3111 (1994).
[9] S. Sakane, W. Liu, D. J. Doren, E. L. Shock, and R. H. Wood, Geochim. Cosmochim. Acta **65**, 4067 (2001).
[10] N. C. Holmes, W. J. Nellis, W. B. Graham, and G. E. Walrafen, Phys. Rev. Lett. **55**, 2433 (1985).
[11] R. Chau *et al.*, J. Chem. Phys. **114**, 1361 (2001).
[12] E. Schwegler, G. Galli, and F. Gygi, Phys. Rev. Lett. **84**, 2429 (2000).
[13] E. Schwegler, G. Galli, F. Gygi, and R. Q. Hood, Phys. Rev. Lett. **87**, 265501 (2001).
[14] C. Cavazzoni, G. L. Chiarotti, S. Scandolo, E. Tosatti, M. Bernasconi, and M. Parrinello, Science **283**, 44 (1999).
[15] E. Katoh, H. Yamawaki, H. Fujihisa, M. Sakashita, and K. Aoki, Science **295**, 1264 (2002).
[16] C. W. F. T. Pistorius, M. C. Pistorius, J. P. Blakey, and L. J. Admiraal, J. Chem. Phys. **38**, 600 (1963).
[17] O. Mishima and S. Endo, J. Chem. Phys. **68**, 4417 (1978).
[18] Y. Fei, H. K. Mao, and R. J. Hemley, J. Chem. Phys. **99**, 5369 (1993).
[19] F. Datchi, P. Loubeyre, and R. LeToullec, Phys. Rev. B **61**, 6535 (2000).
[20] N. Dubrovinskaia and L. Dubrovinsky, High Press. Res. **23**, 307 (2003).
[21] M. R. Frank, Y. Fei, and J. Hu, Geochim. Cosmochim. Acta. **68**, 2781 (2004).
[22] B. Schwager, L. Chudinovskikh, A. Gavriliuk, and R. Boehler, J. Phys.: Condens. Matter **16**, S1177 (2004).
[23] I. M. Chou, J. G. Blank, A. F. Goncharov, H. K. Mao, and R. J. Hemley, Science **281**, 809 (1998).
[24] W. A. Bassett, A. H. Shen, M. Bucknum, and I. M. Chou, Rev. Sci. Instrum. **64**, 2340 (1993).
[25] N. J. Hess and D. Schiferl, J. Appl. Phys. **71**, 2082 (1992).
[26] W. B. Holzapfel, J. Chem. Phys. **56**, 712 (1972).
[27] G. E. Walrafen, M. Abebe, F. A. Mauer, S. Block, G. J. Piermarini, and R. Munro, J. Chem. Phys. **77**, 2166 (1982).
[28] A. Polian and M. Grimsditch, Phys. Rev. Lett. **52**, 1312 (1984).
[29] K. R. Hirsch and W. B. Holzapfel, J. Chem. Phys. **84**, 2771 (1986).
[30] Ph. Pruzan, J. C. Chervin, and M. Gauthier, Europhys. Lett. **13**, 81 (1990).
[31] Ph. Pruzan, J. C. Chervin, and B. Canny, J. Chem. Phys. **97**, 718 (1992).
[32] A. F. Goncharov, V. V. Struzhkin, M. S. Somayazulu, R. J. Hemley, and H. K. Mao, Science **273**, 218 (1996).
[33] A. F. Goncharov, V. V. Struzhkin, H. K. Mao, and R. J. Hemley, Phys. Rev. Lett. **83**, 1998 (1999).
[34] W. R. Busing and D. F. Hornig, J. Phys. Chem. **65**, 284 (1961).
[35] E. Gregoryanz, A. F. Goncharov, K. Matsuishi, H. K. Mao, and R. J. Hemley, Phys. Rev. Lett. **90**, 175701 (2003).
[36] F. E. Simon and G. Glatzel, Z. Anorg. Allg. Chem. **178**, 309 (1929).
[37] J. F. Lin, M. Santoro, V. V. Struzhkin, H. K. Mao, and R. J. Hemley, Rev. Sci. Instrum. (in press).
[38] M. Santoro, J. F. Lin, H. K. Mao, and R. J. Hemley, J. Chem. Phys. **121**, 2780 (2004).
[39] C. S. Zha and W. A. Bassett, Rev. Sci. Instrum. **74**, 1255 (2003).